20
Theoretical Neuroscience of Self-Organized Criticality: From Formal Approaches to Realistic Models

Anna Levina, J. Michael Herrmann, and Theo Geisel

20.1
Introduction

Self-organized criticality (SOC) is a common phenomenon in nature [1] and became a fascinating research subject for neuroscience when critical avalanches were predicted theoretically and observed experimentally to occur in networks of neurons [2–4]. Models of SOC in neural network evolve from early sandpile-like models [5, 6] on a lattice to large-scale realistically connected networks [7, 8]. In this chapter we will present a model of criticality in the brain which identifies a number of contributing factors such as short-term synaptic dynamics and homeostatic plasticity in the synapses. This model is but one approach among an ever-increasing number of other studies on the subject. We were aiming for a family of models that are simple enough to permit an analytical solution but can still account for several biological principles that are known to be relevant here.

As we try to identify the components of a neuronal network that can make it self-organized critical or, at least, bring it closer to a critical state, we have to be aware that criticality (in the sense of the existence of full-fledged power law event distributions) does not exist in finite systems. This emphasizes the importance of analytical treatments for infinite systems, while a theory of finite-size effects is also required to relate precisely to biological experiments. Such a theory exists only for the simplest abstract models (see Section 20.2), which forces us to apply a combination of analytical and numerical work on models including dynamic synapses (Section 20.3) and homeostatic adaptation (Section 20.4).

20.2
The Eurich Model of Criticality in Neural Networks

In 2002, Eurich *et al.* [2] presented a model of a globally coupled neural network that exhibits critical avalanches. In contrast to earlier work on criticality [5, 6, 9–11], here an explicit analytical derivation of the distribution of sizes of neural avalanches was given not only for the idealization of very large networks but

Criticality in Neural Systems, First Edition. Edited by Dietmar Plenz and Ernst Niebur.

also for networks of any size. This work also predicted the correct critical exponent as well as various extra-critical dynamical phenomena that were later confirmed in neurophysiological experiments [3].

The analytical solvability of the model required a certain degree of simplicity which seems justified, however, by the predictive power of the model. Moreover, details of the model assumptions do not influence the qualitative behavior, which is characteristic of critical phenomena.

20.2.1 Model Description

The model consists of a set of N identical neurons each of which is characterized by a single state variable h representing the neural membrane potential. Depending on the state of the system at time t, a neuron, say neuron i, receives external input $I_i^{\text{ext}}(t)$ or internal input $I_i^{\text{int}}(t)$ from other elements. If the potential h exceeds a threshold θ, the neuron emits an action potential and returns to its resting value h_{rest} which we set for convenience to be equal to 1. The action potential serves as input to the other neurons and increases their membrane potentials by a fixed amount, which in turn may or may not surpass the threshold, thus causing further action potentials. Such a shorter or longer sequence of neural firings forms a neural avalanche in the model. It stops if no neuronal potential is above threshold after the transmitted action potentials have arrived. Time is measured in discrete steps, $t = 0, 1, 2, \ldots$, and action potentials are assumed to travel for a single time step only. The system is initialized by arbitrary values h_i, $i = 1, \ldots, N$, in the interval $[h_{\text{rest}}, \theta)$ which we choose conveniently as $[0, 1)$. We can describe the dynamics of the membrane potential as an accumulation of input that is occasionally interrupted by resets to the resting level after firing.

$$h_i(t+1) = \begin{cases} h_i(t) + I_i^{\text{int}}(t) + I_i^{\text{ext}}(t) & \text{if } h_i(t) + I_i^{\text{int}}(t) + I_i^{\text{ext}}(t) < 1 \\ h_i(t) + I_i^{\text{int}}(t) + I_i^{\text{ext}}(t) - 1 & \text{otherwise} \end{cases} \tag{20.1}$$

The internal input $I_i^{\text{int}}(t)$ is the product of the synaptic strength α and the number $\xi(t)$ of action potentials generated in the current time step, $I_i^{\text{int}}(t) = \alpha\, \xi(t)/N$, where we use the assumption of identical synapses for all neurons. The interaction strength $\alpha \geq 0$ is the only adjustable parameter in the model. It determines the synaptic efficacy between any two neurons. The scale $1/N$ ensures that a neuron receives comparable amounts of input independently of the size of the network.

The external input effects a ''charging'' of the neural elements and is realized by randomly selecting a single neuron in each time step and adding a small increment $I_i^{\text{ext}}(t) = \Delta h$ to its membrane potential. Another option would be spontaneous activity, that is, setting the potential of a random neuron to a superthreshold value.

We assume that avalanches start always with a single firing event, that is, $\xi(t_0) = 1$. Other neurons may be incited to fire as well, but it is also possible that no other neurons join in. Thus the avalanche always has a *size* greater than or equal to 1. Formally, the avalanche size L is the sum over the sets of active

neurons, $L = \sum_{k=0}^{D-1} \xi(t_0 + k)$ over the *duration* D of the avalanche. The duration is the smallest integer for which the stopping condition $\xi(t_0 + D) = 0$ is satisfied.

One of the important advantages of the model [2] is that the probability $P(L, N, \alpha)$ of an avalanche of size L in a network of N neurons can be calculated explicitly for each coupling parameter α.

$$P(L, \alpha, N) = L^{L-2} \left(\frac{N-1}{L-1}\right) \left(\frac{\alpha}{N}\right)^{L-1} \left(1 - L\frac{\alpha}{N}\right)^{N-L-1} \frac{N(1-\alpha)}{N-(N-1)\alpha} \qquad (20.2)$$

This probability distribution has been introduced by Eurich *et al.* [2] and was analyzed by Levina [12], where also the name *Abelian distribution* was proposed because of the fact that an Abelian sum is involved. In the following section, we will compare the results of the analysis of the model based on Eq. 20.2 with numerical simulations [2].

20.2.2 Simulations and Analysis

Depending on the connection strength α, the network can produce a rich repertoire of behaviors, see Figure 20.1. For small values of α, the behavior is subcritical, that is, the avalanche size distribution decays exponentially and the number of avalanches that extend to the size of the system is negligible. If α equals the critical value α_{cr}, the system has an approximate power law avalanche distribution with an exponent close to $-3/2$ for avalanche sizes almost up to the system size where an exponential cutoff takes place. The distributions become nonmonotonous in the region $\alpha_{cr} < \alpha < 1$. For α just below 1, neurons can fire more than once per

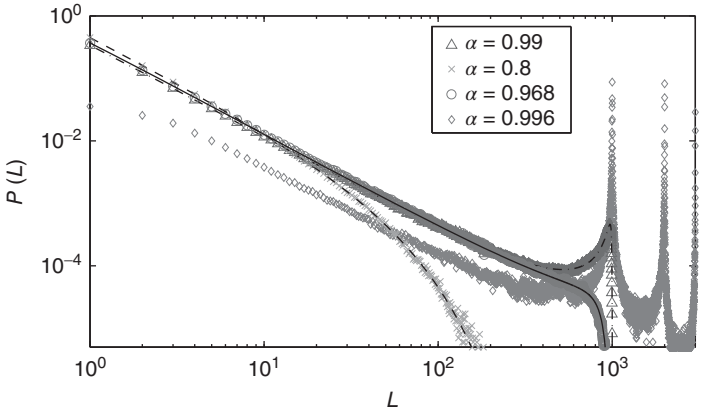

Figure 20.1 Probability distributions of avalanche sizes, $P(L, \alpha, N)$, in the subcritical (stars, $\alpha = 0.8$), critical (circles, $\alpha = 0.968$), supercritical (triangle, $\alpha = 0.99$), and multi-peaked (diamonds, $\alpha = 0.996$) regime. Thin lines denote the analytical results for the avalanche size distributions. The symbols show temporal averages from simulations of 10^6 avalanches with $N = 1000$ and $\Delta h = 0.02$.

avalanche such that avalanche sizes larger than N are possible. Finally, if $\alpha \geq 1$, then the activity in the network will never terminate once an avalanche of size at least N has occurred.

The exact formula (20.2) allows us to determine the critical connection strength in the thermodynamic limit. Note that here several limits are involved: First, the limit of large system size $N \to \infty$ is taken. Then we let $\alpha \to 1$, and, finally, in order to justify the power law

$$P(L) \propto L^{-\frac{3}{2}}$$

we need also to consider large L because Stirling's approximation implies a weel correction for small L.

The case $\alpha = 1$ is special because it implies the conservation of the neural activity in the thermodynamic limit. Numerous authors have presented arguments against the existence of nonconservative SOC models [10, 13–15] or proposed variants that were claimed to be critical in nonconservative cases [8, 16, 17]. For example, for the Abelian sandpile (i.e., a system where dynamics does not depend on the order of the update of the nodes) it was proven that conservation is necessary for SOC [18], but so far there is no final conclusion of this discussion, although the known SOC systems are conservative. In this context, it is interesting that, in the Eurich model, for $N < \infty$, the distributions that are closest to a power law occur at $\alpha_{cr} < 1$.

The restrictions of this model do not allow for a functional description of biological neuronal avalanches [3] because the parameter α needs to be tuned appropriately and, with increasing system size, more and more precisely. In real neural systems, however, critical behavior appears to be typical [19–21], and is assumed to arise from some form of feedback, which has been indicated to be essential for SOC in a general context [22]. In the next section we will introduce an extension of the model that includes such a feedback mechanism.

20.3 LHG Model: Dynamic Synapses Control Criticality

In this section we will describe an extension of the Eurich model which includes an activity-dependent dynamics of the synaptic weights. It was proposed by the present authors [23] and is sometimes referred to as the *LHG model* [24, 25].

20.3.1 Model Description

The essential difference to the previous model is that the synaptic strengths are no longer kept fixed but are allowed to follow now an activity-dependent dynamics. The synapses are described by individual variables, while α sets the scale for the maximal synaptic strength or, more biologically, the total amount of neurotransmitter in a synapse. After a presynaptic spike, the increase of the potential of the postsynaptic neuron is given by $uJ_{ij}(t)$, where $J_{ij}(t)$ stands for the amount of synaptic resources

that are available at time t in a synapse between neurons j and i, and u is the fraction of these resources that is actually used for a transmission. Avalanches and model details are defined in the same way as before, and the dynamics of the membrane potential is described analogous to Eq. 20.1, but in differential form and with ζ denoting the random driving inputs and with a synaptic delay τ_d.

$$\dot{h}_i = \delta_{i,\zeta(t)} I^{\text{ext}} + \frac{1}{N} \sum_{j=1}^{N} u J_{ij} \delta \left(t - t^j_{\text{sp}} - \tau_d \right) \tag{20.3}$$

The dynamics of the variables J_{ij} represents the effect of synaptic depression [26]

$$\dot{J}_{ij} = \frac{1}{\tau_J} \left(\frac{\alpha}{u} - J_{ij} \right) - u J_{ij} \delta \left(t - t^j_{\text{sp}} \right) \tag{20.4}$$

and combines two effects. First, a synapse decreases in strength by a fraction u when activated because of a depletion of the resources of synaptic transmitters. Second, it slowly recovers and reapproaches the scaled maximal value $\frac{\alpha}{u}$ when the neuron is silent. Thus, if the firing frequency is low (e.g., less than one spike in 50 time steps), then the synapse has enough time to return close to the maximal value. If the frequency is higher, then the synaptic strength at firing is smaller than maximally possible [26]. If a neuron spikes rarely, the synaptic strength uJ_{ij} approaches α. The fraction u is fixed here, but it may as well be affected by the neural activity (cf. Section 20.3.4). Here we should include a remark relating to the separation of time scales in the model. Between avalanches, the network receives external inputs at a rate $1/\tau_s$: that is, each neuron receives on average an external input every $N\tau_s$ milliseconds. In the simulation we are free to rescale the time during these intervals and choose conveniently τ_s as a discretization step. The timescale τ_J in Eq. 20.4 is related to this rate by $\tau_J = \nu N \cdot \tau_s$, which gives rise to another parameter of the model, ν, which is chosen to maintain a compromise between the timescale separation and the continuity of the physiological processes underlying the synaptic dynamics (Eq. (20.4)).

Just as in Section 20.2, finite networks show different avalanche size distributions for different values of α (see Figure 20.2), ranging from subcritical at small values of α to supercritical for large α. Near α_{cr}, the system has an approximate power law distribution of avalanche sizes. Here, however, the situation is more interesting as the range of near-criticality changes with the number of neurons (see Figure 20.3) and becomes dominant in the limit of large N as we will show in Section 20.3.2. To verify this claim numerically, we have used the method of finite-size scaling [27–29], details of which are given by Levina [12]. In order to quantify the difference between the models, we define a threshold $\vartheta = 0.005$ describing a ''very good fit''[1] and compare the parameter regions that deliver a critical distribution with at least this quality. The difference between the static model and the dynamic model is one order of magnitude (see inset in Figure 20.3). The result does not depend on the particular value of ϑ as long as it is not too large. In contrast to the static case, the

1) Meant in the sense of a linear regression of the logarithms, but other estimates have been tested as well.

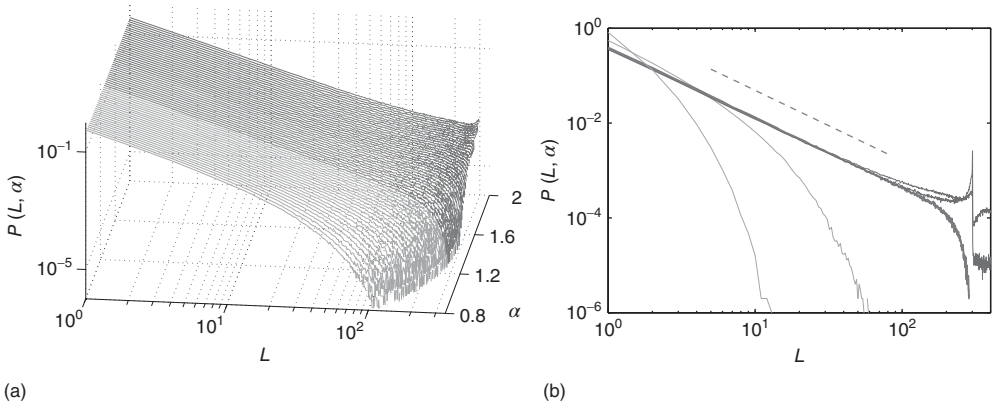

Figure 20.2 Distribution of avalanche sizes for different values of the connection parameter α. (a) At $\alpha < 1.3$, the distribution is subcritical (green). It becomes critical in an interval around $\alpha = 1.4$ (red). For $\alpha > 1.6$, the distribution is supercritical (blue). (Figure first published in Ref. [23].) (b) Characteristic examples of all three kinds of distributions with the same color code. Results are obtained for $N = 300$, $\nu = 10$, $u = 0.2$, $I^{\text{ext}} = 0.025$ (Figure adapted from Ref. [39].) http://www.nature.com/reprints/permission-requests.html. (Please find a color version of this figure on the color plates.)

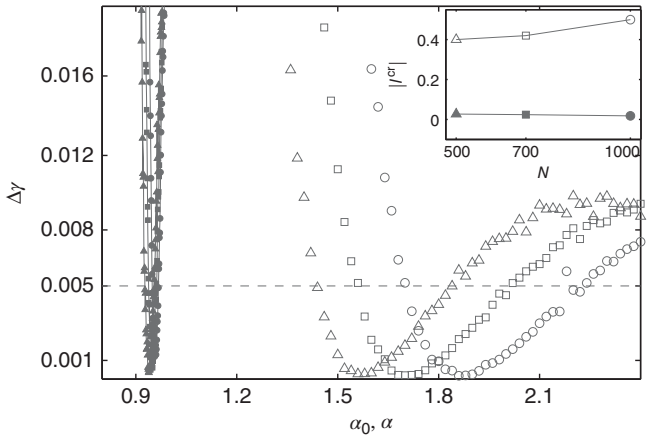

Figure 20.3 The range of connectivity parameters where critical events extend to the system size. The mean-squared deviation $\Delta\gamma$ from the best matching power law is plotted as a function of α. Empty circles, squares, and triangles stand for networks with dynamic synapses and system sizes $N = 500$, 700, and 1000, respectively. The results are based on a number of avalanches that scale with N^2. Filled symbols represent the static model. The inset (same symbols) shows the lengths of the parameter intervals where the deviation from the best matching power law is smaller than 0.005. (Figure first published in Ref. [23].)

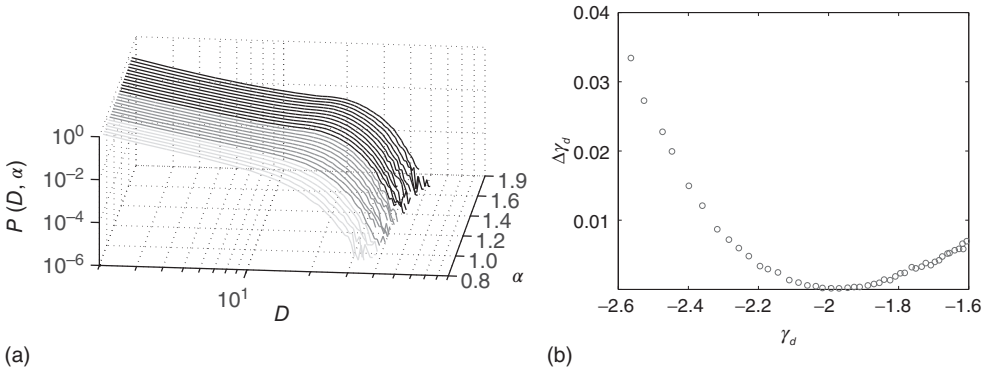

Figure 20.4 (a) Avalanche duration distribution for different values of the connectivity parameter α. (b) Power law exponent γ_d fitted for small avalanche durations as a function of the goodness of the power law fit to the avalanche size distribution. $N = 100$, $\nu = 10$, $u = 0.2$. In (a), green gray traces correspond to subcritical distributions of avalanche sizes, red gray traces critical and blue ones supercritical. For details see Figure 20.2. (Please find a color version of this figure on the color plates.)

critical region with dynamic synapses apparently increases with the system size. The power law exponent at criticality for finite networks has a smaller modulus than −1.5, but it approaches this value in the limit.

The avalanche duration distributions deviate strongly from a power law for durations larger than 10, that is, they consist mainly of the exponential cutoff (cf. Figure 20.4(a)). We determined the slope of the power law by fitting the region of short durations where a power law is still applicable. Similar to the experimental findings [3], the exponent for the critical duration distribution is found to be −2 (cf. Figure 20.4(b)).

20.3.2 Mean-Field Approximation

The above discussion, as well as biological evidence, suggests that the synaptic strength is an important factor for the avalanche size. We will now consider a relation between α and the effective synaptic strength and derive a large N approximation for the resulting avalanche size distribution in the critical case.

The mean-field assumption stipulates that we can consider the mean $u\langle J_{ij}\rangle$ instead of the full distribution of synaptic strengths across the network. Obviously, the dynamic network is now comparable to a static model with $\alpha = u\langle J_{ij}\rangle$, which is also evident from numerical simulations [23]. We can thus rely on the results from the static case (Eq. (20.2)), but have to take into account that $\langle J_{ij}\rangle$ is no longer a free parameter but depends in turn on the avalanche distribution.

In order to express the average synaptic strength analytically, we refer to the average inter-spike interval Δ^{ISI} of a neuron (which is usually larger than the inter-avalanche interval). The relation between Δ^{ISI} and $\langle J_{ij}\rangle$ involves a form of regulation: If the inter-spike intervals are short, then the synapses have a short

time to recover and the average synaptic strength resides at a low level, while large synaptic strengths lead more often to long avalanches and to large inputs to neurons during the avalanches, which tends to shorten inter-spike intervals. This trade-off determines the effective synaptic strengths and the inter-spike intervals that are realized by the dynamics of the network. In order to express this formally, we solve the dynamical equations (20.3) and (20.4) and obtain the following equations [12, 23]:

$$\langle J_{ij} \rangle = G\Big(\langle \Delta^{\mathrm{ISI}} \rangle\Big) \tag{20.5}$$

$$\langle \Delta^{\mathrm{ISI}} \rangle = F\Big(\langle J_{ij} \rangle\Big) \tag{20.6}$$

The above equations must hold simultaneously and represent a self-consistency requirement in our approach. Because both F and G are increasing functions, the solution is unique; it agrees perfectly with numerical simulations [23].

With increasing N, the stationary distribution becomes less and less sensitive to changes of the parameter α near the critical value, which brings about the large critical region for the LHG model. The growth of the ''critical interval'' with the system size (Figure 20.3) can be rigorously shown in the thermodynamic limit. For $N \to \infty$, the region extends from $\alpha = 1$ to infinity while the deviation from an ideal power law vanishes.

The stability of the solution of the self-consistency equations (20.6) and (20.6) can be demonstrated based on the following idea. Applying a positive perturbation $\Delta J > 0$ to all synapses at time t_{p} leads to a temporary increase of the avalanche size. The average size of a few avalanches following t_{p} will be larger than in the unperturbed case. This leads, on average, to a decrease of the inter-spike intervals, which affects the average synaptic activity. The average synaptic strength at the time of the second spike after perturbation can be found from Eq. (20.4), and it can be shown that positively perturbed synapses decrease their strength to return to the equilibrium state. The same argument shows that negatively perturbed synapses increase their strength thus counteracting the perturbation.

20.3.3
Toward a Realistic Model: Network Structure, Leakage, and Inhibition

The analysis in the previous sections was considerably simplified by the restrictive model assumptions. As a side effect, this allowed us also to separate certain effects from each other. For example, for complete connectivity, effects due to the internal neural adaptation are distinguishable from network effects. See, for example, the work by Lin and Chen [30] and Teramae and Fukai [31], where often small-world connectivity is found to contribute to criticality.

We will ask here how the combination of specific connectivity and depressive synapses shapes the statistics of the network dynamics. To start with, let us consider a simple random connectivity scheme. Each neuron is connected to $p_1 N$ randomly selected neurons. Such a random network is statistically homogeneous and connected if p_1 is large enough (e.g., $p_1 \approx 0.2$). Therefore, the mean-field

approximation is still valid. The critical regime can be identified by rescaling α, where the new critical connectivity strength is now $\alpha_{cr}(N)/p_1$, where $\alpha_{cr}(N)$ is the critical parameter of a fully connected network of size N.

We will also consider another type of a random network where the degree of the nodes is not restricted. Instead of the above neuron-based procedure, we connect any pair of neurons with the same probability p_2.

As a more general setup, we study the avalanche dynamics in a small-world network [32] which can be tuned by a parameter in between the extreme cases of a regular nearest-neighbor connectivity and a purely random network.

Comparing the four types of connectivity (nearest neighbors, two random networks, and small-world connectivity, each with appropriately rescaled parameters), we find significant differences (see Figure 20.5). Although the dependence of the critical exponent on the maximal synaptic strength α has a similar shape, the slopes are different and are steepest for the nearest-neighbor connectivity. This is reflected also in the deviation from the best matching power law, which again is largest for the regular network. Independently of the particular choice of the criterion for criticality in a finite system, the region corresponding to the random

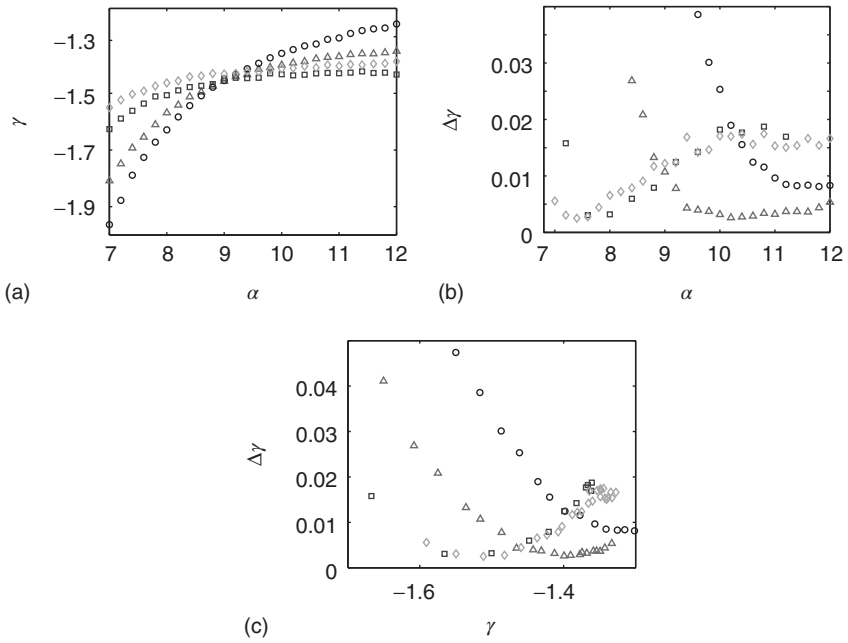

Figure 20.5 Comparison of different connectivity schemes. (a) Exponent of the best matching power law for different αs. (b) Deviation from the best matching power law for different αs. (c) Deviation from the best matching power law as a function of the matched exponent. Different symbols stand for different connectivities: circles – nearest neighbors, triangular – small-world, squares – random connectivity with fixed number of connection per neuron, diamonds – random connectivity. Parameters are $N = 500$, $\nu = 10$, $u = 0.2$, average connectivity is always 20%.

network with a fixed number of connections per neuron is smaller than for the unrestricted random network, which in turn is smaller than the critical region for the small-world network. Small-world networks show thus a tendency to ''improve'' the power law in the sense that the deviation between the observed distribution and the best matching power law decreases (Figure 20.5).

Another assumption in the LHG model is the perfect integration, that is, the neurons are nonleaky integrators. In contrast to the examples where the introduction of an arbitrarily small leakage to the model neurons destroys the results for a leak-free system (see, e.g., [33, 34]), small leakage does not destroy the power law avalanches. Instead of Eq. (20.3), we now use the following dynamics for the membrane potentials:

$$\dot{h}(t) = -\frac{1}{\tau}h(t) + C + I^{\text{ext}} + I^{\text{int}}$$

where the variable C stands for an active process, for example, a dynamic threshold, that compensates the leak currents. In this way, the neurons can remain close to the threshold and the network remains conservative.

The avalanche size distribution (Figure 20.6) does not change when a moderate leakage is introduced. The power law exponent becomes larger in magnitude, reaching approximately −1.9. Strong leakage, however, suppresses power laws in the present model.

Finally, we want to consider the effect of inhibitory synapses in the model which was so far all-excitatory. It is known that inhibition often leads to synchronization in neuronal networks, which in turn could interfere with critical behavior. It is natural to introduce inhibition according to Dale's principle (which states that neurons release the same set of transmitters at all of their synapses) [35, 36]. Accordingly, we select a fraction of neurons [37] and change the signs of their synaptic strengths. After integrating both excitatory and inhibitory inputs to a neuron, we require that the membrane potential remains positive, that is, we set $h = 0$ if the inhibition

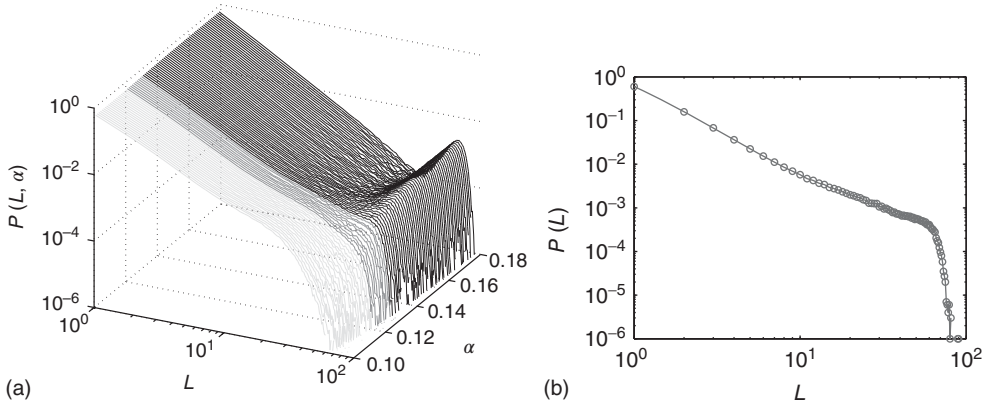

Figure 20.6 Distribution of avalanche sizes in a network with leaky neurons for different values of the connectivity parameter α (a) and for the critical case ($\alpha = 0.125$) (b) $N = 100$, $C = 0.98$, $\tau = 40$ ms.

dominates. In addition, we will also model inhibition by a randomization of the signs of synaptic strengths without enforcing Dale's principle. In both cases, a portion of 0.2 of all synapses will have negative sign [37].

Figure 20.7 shows the avalanche size distributions for the two types of inhibition. If Dale's principle holds, an externally activated neuron is inhibitory with probability of 0.2, such that avalanches of size 1 are relatively more frequent, a fact which violates the power law at small avalanche sizes but is irrelevant for the critical behavior because only the asymptotics is relevant and the inhibition has no effect for larger avalanches. In both cases, the power law exponents are approximately −1.5 in the critical regime (with Dale's principle about −1.47, without about −1.52). We thus conclude that inhibition does not interfere with the critical behavior.

20.3.4 Synaptic Facilitation

Depressing synapses can regulate the network dynamics toward criticality. Some synapses experience also an activity-dependent facilitation at a shorter timescale than the depression. We show, that criticality is achieved in the network with facilitatory synapses in a self-organized way [38, 39].

Facilitation enters the model via the "usage" parameter u in Eq. (20.4). The synaptic model [40, 41] posits an activity-related increase of the fraction of synaptic resources that are used in the transmission. In the scheme adopted here, an action potential causes the respective individual usage variables u_{ij} to increase. After the spike, they decrease again with a time constant τ_u. The corresponding kinetic equation

$$\dot{u}_{ij} = \frac{1}{\tau_u}(u_0 - u_{ij}) + (1 - u_{ij})u_0\delta\left(t - t^j_{\mathrm{sp}}\right) \tag{20.7}$$

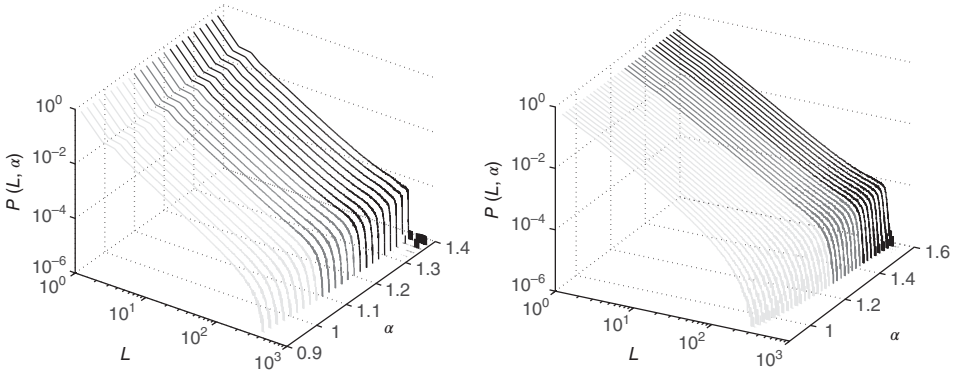

Figure 20.7 Network with 20% inhibitory connections (a) with and (b) without Dale's principle. The avalanche size distribution is plotted for different αs. For the plot on the left, only avalanches of size 6 or larger were used in the estimation of the power law exponent. $N = 500$, $\nu = 10$, $u = 0.2$.

describes the dynamics of the parameter u in Eq. (20.4) for each synapse individually. The parameter u_0 in Eq. (20.7) denotes the minimal fraction of the synaptic resources that are used for a spike. The two equations (20.4) and (20.7) together with the membrane potential dynamics equation (20.3) govern the behavior of this model neural network.

The size distributions for finite networks show again subcritical, critical, and supercritical regimes for different values of α (Figure 20.8). Below a first critical value α_{cr}, the network is always subcritical, and above a second critical value $\alpha^{cr} > \alpha_{cr}$, supercritical behavior can be observed. In between the two critical values, the system has an approximate power law avalanche distribution for a large volume of initial conditions. The subcritical branch persists as well in the interval $[\alpha_{cr}, \alpha^{cr}]$ (Figure 20.8). This implies a hysteretic behavior, which is illustrated by Figure 20.9.

If α is smaller than α_{cr}, there is only one solution of the self-consistency equation. At $\alpha = \alpha_{cr}$, a saddle–node bifurcation creates a stable and an unstable branch in addition to the existing stable branch. In between α_{cr} and α^{cr}, three solutions coexist, of which two are stable; Finally, at $\alpha = \alpha^{cr}$, a second bifurcation occurs where the subcritical branch and the unstable branch annihilate such that for larger α only a single solution remains (Figure 20.9). The simulations indicate that the range of criticality increases with system size, and eventually all values of $\alpha > \alpha_{cr}$ are critical. This can be shown analytically in a similar way as for the purely depressive network. The lower boundary of the critical region for an infinite network is given by $2\sqrt{u_0 - u_0^2} \leq 1$, that is, facilitatory synapses extend the critical region toward lower synaptic strengths.

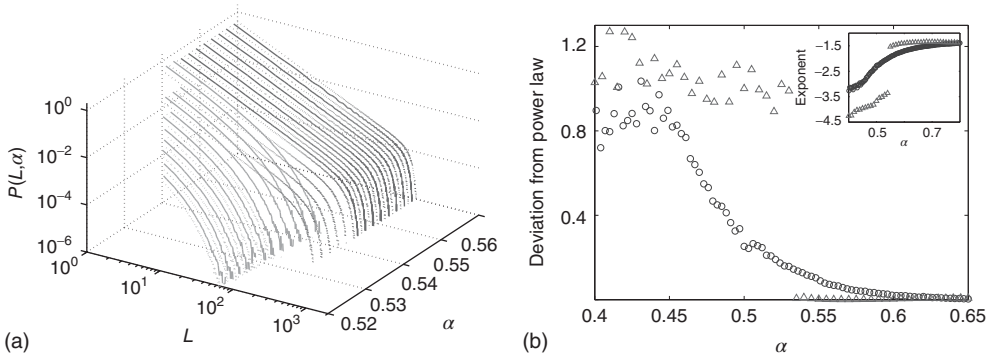

Figure 20.8 (a) Distribution of avalanche sizes for different values of α. Below $\alpha < 0.543$, a subcritical distribution exists (green). Critical behavior can be observed above $\alpha = 0.53$ (blue/red). The picture indicates a hysteresis with respect to α, which is illustrated by the section through the 3-D plot and shown in the inset. For large networks, all distributions of the upper branch are critical, while the lower branch remains subcritical. See also Figure 20.9. (b) Deviation of avalanche size distribution from a power law for different α. Triangles represent facilitatory synapses, while circles represent depressing synapses. The inset shows the exponent of the nearest power law distribution. For both, $N = 300$, $\nu = 10$, $u_0 = 0.1$, $I_0 = 7.5$ [39]. (Copyright 2009 by The American Physical Society). (Please find a color version of this figure on the color plates.)

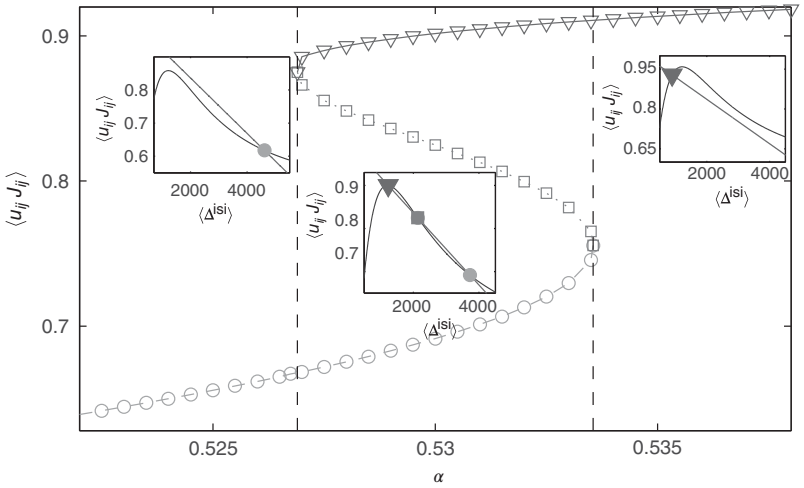

Figure 20.9 Bifurcation diagram representing the solutions of the self-consistency equation for the model with facilitating and depressing synapses. The average interaction strength $\langle u_{ij} J_{ij} \rangle$ is plotted against the interaction parameter α. The insets show the graphical solutions of the self-consistency equation which may have one or three solutions here, in contrast to the purely depressive case (Eqs. (20.5) and (20.6)) where a unique solution exists. $N = 300$, $\nu = 10$, $u_0 = 0.1$, $I_0 = 7.5$. The bifurcation points are at $\alpha_{cr} = 0.534$ and $\alpha^{cr} = 0.547$. Modified from [39].

We have proposed [39] that the coexistence of a critical and a subcritical phase in this model may be related to the phenomenon of "up" and "down" states in the prefrontal cortex, an idea that was later elaborated by Millman *et al.* [8].

20.4 Criticality by Homeostatic Plasticity

Neuronal avalanches are homeostatically regulated, which has been demonstrated recently by Plenz (2012) [42], where networks after being perturbed away from the critical state gradually, within hours, return to criticality. This suggests a slow adaptation process which we will study in this section.

20.4.1 Branching Processes

The Galton–Watson branching processes were introduced in 1874 to explain the disappearance of some of the British family names [43]. Since then, they were extensively studied in mathematics [44, 45] and applied in biology and physics [46].

A branching process generates tree-like structures where each node produces i descendants with a probability p_i. The fact that the probability does not depend on the events in earlier generations differs from the situation in neural networks

where the effectiveness of a spike depends on their recent activity. Nevertheless, it was shown that branching processes provide a good approximation for data obtained from multielectrode recordings [47].

The evolution of an avalanche can be described, similar to a branching process, by the temporal sequence $\{\xi_t\}$ of the activity levels in the network. The neural connectivity parameter α corresponds to the branching parameter α_{br} of a Galton–Watson process, which describes the average number $\sum_i ip_i$ of offspring per node. The stochasticity of the process is brought forth by the randomness of the external inputs in between the avalanches. But, since the driving is assumed to halt during avalanches, the sequence ξ_t is deterministic for all $t < D$.

The sequence of neural activity $\{\xi_t\}$ is still different from a branching process because it does not share the Markov property of branching processes. That is, because of the condition $\xi_t \leq N - \sum_{s=1}^{t-1} \xi_s$, the value of ξ_t depends not only on the preceding value ξ_{t-1} but also on all previous activations during the avalanche.

Interestingly, for large networks this difference becomes irrelevant: that is, if the network size tends to infinity, then the distribution of the neural firings $\{\xi_t\}_{t=1}^{\infty}$ approaches the distribution of a Galton–Watson branching process [12, 48]. This asymptotic relation requires, however, that the membrane potentials are evenly spread across the phase space of the system, that is, the states of the neurons become more and more uniformly distributed independent of the initialization and in spite of the partially synchronizing effects of the ongoing avalanches. Such mixing properties can be shown by simulations, and the related analytical results have been obtained [12].

In this way, we can use the results from branching theory for control of the network. In particular, it is known [49] that the avalanche sizes in a critical branching process, that is, for $\alpha_{\mathrm{br}} = 1$, are distributed as $P(\xi = L) \propto L^{-\frac{3}{2}}$, which can be used to derive a local learning rule that induces criticality.

20.4.2 Self-Organization by Long-Term Plasticity

A learning rule for criticality can be obtained by enforcing conservation of neural activity and thereby generating an approximation of a branching process. In particular, for the beginning of an avalanche we will require that on average only one more neuron gets activated:

$$E_i(t) = \begin{cases} \frac{1}{2}\left(\sum_j S_j(t) - 1\right)^2 & \text{if } S_i(t-1) = 1 \\ 0 & \text{otherwise} \end{cases} \tag{20.8}$$

The criterion is not implausible because in a globally or randomly coupled network the total activity $\sum_i S_i(t)$ can be estimated locally from the internal input at the next time step. Eq. (20.8) gives rise to a learning rule for the synaptic strength [48]:

$$\alpha^{t+1} = \alpha^t + \varepsilon_{\mathrm{homeo}} \left(1 - l - N^{-\frac{1}{2}}\right) \tag{20.9}$$

where l is the activity at the following time step and $\varepsilon_{\mathrm{homeo}} \ll 1$ is a learning rate. Eq. (20.9) reduces the synaptic weight if the activity tends to increase and reduces

it otherwise: that is, learning according to Eq. (20.9) is *homeostatic* [50] because it tends to stabilize the flow of neural activity. A similar learning rule has been studied in Boolean networks [51], where also deviations from the ideally critical behaviors were noticed. Here they may be caused by the difference to a branching process for finite networks.

Because the number of neurons that respond to a single spike is bounded, the branching parameter tends to be underestimated. To compensate for this effect, we include a finite-size correction into Eq. (20.9). As a result (see Figure 20.10), the synaptic weights converge to the value that was identified as the critical value for finite system sizes of a network with static synapses (Eq. (20.2)).

The avalanche dynamics together with the slow homeostatic learning drives the system to a critical state independently of the initial conditions such that the neuronal network with this learning rule is indeed self-organized critical.

20.4.3
Effects of Spike-Time-Dependent Plasticity and Network Structure

The structure of neural networks is a product of developmental processes as well as activity-dependent learning (spike-time dependent plasticity, STDP, see [52]), which in combination with the short-term synaptic dynamics and homeostatic effects determines the activity dynamics. This raises the question how the complex interaction of these contributions interferes with criticality. The following sections present some evidence for cooperativity: that is, the effects are found to support each other in the maintenance of a critical regime.

We now consider a network with synaptic weights that are composed of three factors, each of which evolves on a different timescale.

$$w_{ij} = uJ_{ij}w_{ij}^{\mathrm{STDP}}w_{ij}^{\mathrm{h}} \tag{20.10}$$

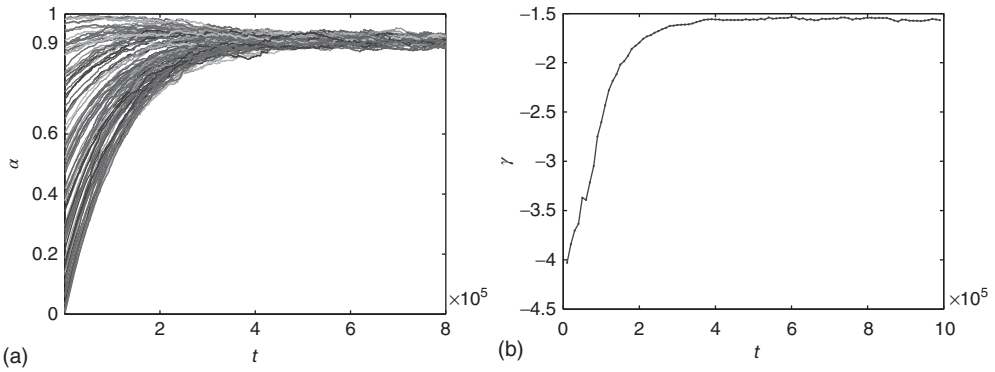

Figure 20.10 (a) Homeostatic learning of individual synapses. Shown are trajectories of the synaptic strengths of a single neuron during the initial learning phase. (b) The exponent of the power law fit to the avalanche size distribution during homeostatic learning clearly approaches the critical value of $-3/2$. $N = 100$, $T \leq 2 \cdot 10^6$, $\varepsilon_{\mathrm{homeo}} = 10^{-4}$ [48].

The variables J_{ij} follow the short-term dynamics (Eq. (20.4)), w_{ij}^{h} are governed by the homeostatic learning rule (20.9), and w_{ij}^{STDP} are subject to STDP learning:

$$\Delta w_{ij}^{\mathrm{STDP}} = \begin{cases} \epsilon_{\mathrm{STDP}} \left(1 - \dfrac{w_{ij}^{\mathrm{STDP}}}{W_{\max}}\right) e^{t_j^{\mathrm{sp}} - t_i^{\mathrm{sp}}} & \text{if } t_i^{\mathrm{sp}} > t_j^{\mathrm{sp}} \\ -\epsilon_{\mathrm{STDP}} \dfrac{w_{ij}^{\mathrm{STDP}}}{W_{\max}} e^{t_j^{\mathrm{sp}} - t_i^{\mathrm{sp}}} & \text{otherwise} \end{cases} \tag{20.11}$$

Here, t_i^{sp} denotes the time of the last spike of neuron i. The form of Eq. (20.10) is reasonable because homeostatic learning is known to be multiplicative [50] and the STDP rule is used in a multiplicative form. The results do not change if we combine the STDP term w^{STDP} additively, that is, $w_{ij} = uJ_{ij}w_{ij}^{\mathrm{h}} + w_{ij}^{\mathrm{STDP}}$.

Figrue 20.11 presents the results for the individual contributions for a random network with connection probability $p = 0.3$. The network with STDP has a slightly increased critical region which is shifted to the right due to pruning. Homeostatic regulation again produces criticality independently of the parameter α.

To evaluate the impact of the combination of STDP and homeostatic learning, we compare three different scenarios: A network with STDP and homeostatic learning where synaptic dynamics described by Eq. (20.10); a network with homeostatic learning only; and a network with homeostatic learning that was also corrected for pruning to simplify comparison with STDP. In the last case, we measure how many synapses were pruned in the STDP simulation and then delete randomly the same number of synapses from the network before starting with the homeostatic regulation. The results of this comparison are represented in Figure 20.12. The

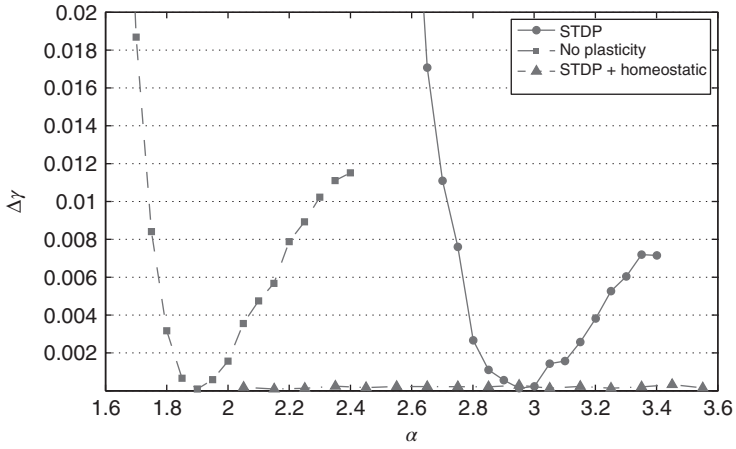

Figure 20.11 Deviation from the best matching power law for different combinations of plasticity rules. Squares: only depressing synapses, circles: depressing synapses and STDP, triangles: depressing synapses and STDP as well as homeostatic regulation. $N = 100$, $W_{\max} = 1.5$, $\epsilon_{\mathrm{homeo}} = 0.01$, $\epsilon_{\mathrm{STDP}} = 0.08$.

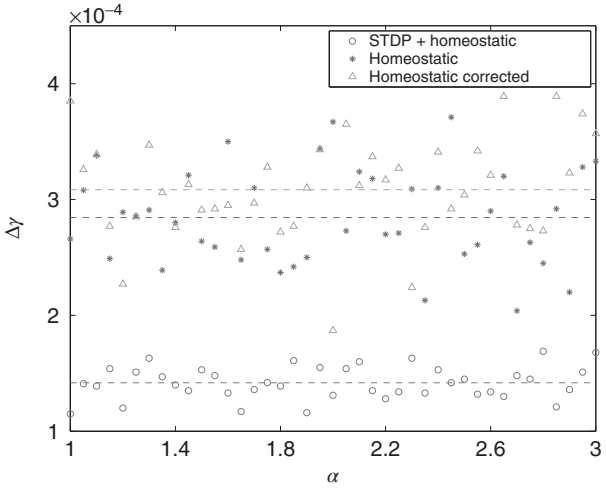

Figure 20.12 Deviation from the nearest power law with and without STDP. Circles: homeostatic plasticity combined with STDP, stars: homeostatic plasticity, asterisks: homeostatic plasticity corrected for pruning. Dashed lines represent averages. $N = 100$, $W_{max} = 1.5$, $\epsilon_{homeo} = 0.01$, $\epsilon_{STDP} = 0.08$.

network with the combination of rules is closer to the critical state independently of the correction for pruning. This result supports the hypothesis that the specific structures that are selected by STDP learning are beneficial for criticality in the network. Similar effects might be responsible for the closeness of the network to a critical state in the models including STDP such as [7].

20.5 Conclusion

The complex dynamics underlying information processing in neural systems is under study from a multitude of approaches. Many phenomena are caused by actively acquired sensory stimuli, feedback from the body, or nonstationary interaction among brain areas. The study of criticality in this context cannot unravel the information processing aspects of brain function, but it can show that the brain has the means to maintain a regime that optimally supports the higher processes. Criticality has been shown to optimize several aspects of brain function such as sensitivity to input, information transmission, and information capacity, for example, by Shew *et al.* [53]. To a physicist, this characterization is reminiscent of the discussion of ground states of physical systems: if the brain was not excited by any internal or external inputs, it would still be critical whenever criticality describes the default behavior of a complex neural system. The fact that the clearest evidence for criticality has been obtained in *in vitro* experiments supports this view.

In addition to some recent results, we have presented the highlights of a journey that took us through the realms of critical systems for more than a decade. While highly simplified systems, such as the Eurich model, may turn out to allow for relevant predictions, most of our work was devoted to a more comprehensive understanding of the function of critical phenomena in physiologically realistic neural systems. Interestingly, the more biological details were included into the series of models, the more closely we arrived to such a functional description of criticality, which in turn represents also a justification of the original approach. Although a large part of the results covered here are due to numerical simulations, it was the analytical study, which we could touch here only briefly, that provided us with the orientation for the development of the models.

Acknowledgment

The authors wish to thank Udo Ernst, Christian Eurich, Tomoki Fukai, Georg Martius, Dietmar Plenz, and Marius Usher for valuable comments, help, and support. They also acknowledge the contributions from Victor Hernandes-Urbina, Sakyasingha Dasgupta, and Maximilian Uhlig. This work was upported by the Federal Ministry of Education and Research (BMBF), Germany, under Grant No. 01GQ1005B.

References

1. Bak, P. (1996) *How Nature Works: The Science of Self-Organized Criticality*, Springer, New York.
2. Eurich, C.W., Herrmann, M., and Ernst, U. (2002) Finite-size effects of avalanche dynamics. *Phys. Rev. E*, **66**, 066–137-06-1–15.
3. Beggs, J.M. and Plenz, D. (2003) Neuronal avalanches in neocortical circuits. *J. Neurosci.*, **23** (35), 11–167.
4. Petermann, T., Lebedev, M., Nicolelis, M., and Plenz, D. (2006) Neuronal avalanches in vivo. *Soc. Neurosci. Abstr.*, **32**, 539.
5. Chen, D., Wu, S., Guo, A., and Yang, Z.R. (1995) Self-organized criticality in a cellular automaton model of pulse-coupled integrate-and-fire neurons. *J. Phys. A: Math. Gen.*, **28**, 5177–5182.
6. Herz, A.V.M. and Hopfield, J.J. (1995) Earthquake cycles and neural reverberations: collective oscillations in systems with pulse-coupled threshold elements. *Phys. Rev. Lett.*, **75**, 1222–1225.
7. Rubinov, M., Sporns, O., Thivierge, J.P., and Breakspear, M. (2011) Neurobiologically realistic determinants of self-organized criticality in networks of spiking neurons. *PLoS Comput. Biol.*, **7** (6), e1002038.
8. Millman, D., Mihalas, S., Kirkwood, A., and Niebur, E. (2010) Self-organized criticality occurs in non-conservative neuronal networks during Up states. *Nat. Phys.*, **6** (10), 801–805. PMCID: PMC3145974.
9. Dunkelmann, S. and Radons, G. (1994) Neural networks and abelian sandpile models of self-organized criticality, in *Proceedings of International Conference Artificial Neural Networks* (eds M. Marinaro and P. Morasso), Springer-Verlag, 867–870.
10. Corral, Á., Perez, C.J., Diaz-Guilera, A., and Arenas, A. (1995) Self-organized criticality and synchronization in a lattice model of integrate-and-fire oscillators. *Phys. Rev. Lett.*, **74**, 118–121.

11. Eurich, C.W., Conradi, T., and Schwegler, H. (1999) Critical and non-critical avalanche behavior in networks of integrate-and-fire neurons, *European Symposium on Artificial Neural Networks*, D-Facto public, Bruges (Belgium), pp. 411–416.
12. Levina, A. (2008) A mathematical approach to self-organized criticality in neural networks. Nieders. Staats- u. Universitätsbibliothek Göttingen. Dissertation (Ph.D. thesis), *webdoc.sub.gwdg.de/diss/2008/levina/levina.pdf*.
13. Grassberger, P. (1994) Efficient large-scale simulations of a uniformly driven system. *Phys. Rev. E*, **49** (3), 2436–2444, doi: 10.1103/PhysRevE.49.2436.
14. Kinouchi, O., Pinho, S.T.R., and Prado, C.P.C. (1998) Random-neighbor Olami-Feder-Christensen slip-stick model. *Phys. Rev. E*, **58**, 3997–4000.
15. Broker, H.M. and Grassberger, P. (1997) Random neighbor theory of the Olami-Feder-Christensen earthquake model. *Phys. Rev. E*, **56** (4), 3944–3952, doi: 10.1103/PhysRevE.56.3944.
16. Olami, Z., Feder, H., and Christensen, K. (1992) Self-organized criticality in a continuous, nonconservative cellular automaton modeling earthquakes. *Phys. Rev. Lett.*, **68** (8), 1244–1247.
17. Lise, S. and Jensen, H.J. (1996) Transitions in nonconserving models of self-organized criticality. *Phys. Rev. Lett.*, **76**, 2326–2329.
18. Tsuchiya, T. and Katori, M. (2000) Proof of breaking of self-organized criticality in a nonconservative abelian sandpile model. *Phys. Rev. E*, **61** (2), 1183–1188, doi: 10.1103/PhysRevE.61.1183.
19. Gireesh, E.D. and Plenz, D. (2008) Neuronal avalanches organize as nested theta-and beta/gamma-oscillations during development of cortical layer 2/3. *Proc. Natl. Acad. Sci. U.S.A.*, **105** (21), 7576.
20. Stewart, C. and Plenz, D. (2008) Homeostasis of neuronal avalanches during postnatal cortex development in vitro. *J. Neurosci. Methods*, **169** (2), 405–416.
21. Tetzlaff, C., Okujeni, S., Egert, U., Worgotter, F., and Butz, M. (2010) Self-organized criticality in developing neuronal networks. *PLoS Comput. Biol.*, **6** (12), e1001 013.
22. Sornette, D. (1992) Critical phase transitions made self-organized: a dynamical system feedback mechanism for self-organized criticality. *J. Phys. I France*, **2**, 2065–2073.
23. Levina, A., Herrmann, J.M., and Geisel, T. (2007b) Dynamical synapses causing self-organized criticality in neural networks. *Nat. Phys.*, **3** (12), 857–860.
24. Bonachela, J.A., de Franciscis, S., Torres, J.J., and Munoz, M.A. (2010) Self-organization without conservation: are neuronal avalanches generically critical? *J. Stat. Mech.: Theory Exp.*, (02), P02 015 *http://iopscience.iop.org/1742-5468/2010/02/P02015/fulltext/*.
25. Choi, H., Maeng, S., and Lee, J. (2012) Self-organized criticality of a simple integrate-and-fire neural model. *J. Korean Phys. Soc.*, **60**, 657–659, doi: 10.3938/jkps.60.657.
26. Markram, H. and Tsodyks, M. (1996) Redistribution of synaptic efficacy between neocortical pyramidal neurons. *Nature*, **382**, 807–810.
27. Kadanoff, L.P., Nagel, S.R., Wu, L., and Zhou, S. (1989) Scaling and universality in avalanches. *Phys. Rev. A*, **39** (12), 6524–6537, doi: 10.1103/PhysRevA.39.6524.
28. Christensen, K. and Olami, Z. (1992) Scaling, phase transitions, and nonuniversality in a self-organized critical cellular automaton model. *Phys. Rev. A*, **46**, 1829–1838.
29. Cardy, J. (ed.) (1996) *Scaling and Renormalization in Statistical Physics*, Cambridge Lecture Notes in Physics, Vol. 5, Cambridge University Press.
30. Lin, M. and Chen, T.L. (2005) Self-organized criticality in a simple model of neurons based on small-world networks. *Phys. Rev. E*, **71**, (016133).
31. Teramae, J. and Fukai, T. (2007) Local cortical circuit model inferred from power-law distributed neuronal avalanches. *J. Comput. Neurosci.*, **22** (3), 301–312.
32. Watts, D. and Strogatz, S. (1998) Collective dynamics of ''small-world'' networks. *Nature*, **393**, 440–442.

33. Gerstner, W. (2000) Population dynamics of spiking neurons: fast transients, asynchronous states, and locking. *Neur. Comput.*, **12**, 43–89.

34. Timme, M., Wolf, F., and Geisel, T. (2002) Prevalence of unstable attractors in networks of pulse-coupled oscillators. *Phys. Rev. Lett.*, **89** (15), 154 105.

35. Dale, H. (1935) Pharmacology and nerve-endings. *Proc. R. Soc. Med.*, **28**, 319–332.

36. Kandel, E., Schwartz, J., and Jessel, T.M. (1991) *Principles of Neural Science*, 3rd edn, Elsevier, New York.

37. Abeles, M. (ed.) (1991) *Corticonics – Neural Circuits of the Cerebral Cortex*, Cambridge University Press.

38. Levina, A., Herrmann, J.M., Geisel, T., Weiss, Y., Scholkopf, B., and Platt, J. (eds) (2006) Dynamical synapses give rise to a power-law distribution of neuronal avalanches, in *Advances in Neural Information Processing Systems 18*, MIT Press, Cambridge, MA. pp. 771–778.

39. Levina, A., Herrmann, J.M., and Geisel, T. (2009) Phase transitions towards criticality in a neural system with adaptive interactions. *Phys. Rev. Lett.*, **102** (11), 118 110.

40. Markram, H., Wang, Y., and Tsodyks, M. (1998) Differential signaling via the same axon from neocortical layer 5 pyramidal neurons. *Proc. Natl. Acad. Sci. U.S.A.*, **95**, 5323–5328.

41. Tsodyks, M., Pawelzik, K., and Markram, H. (1998) Neural networks with dynamic synapses. *Neur. Comput.*, **10**, 821–835.

42. Plenz, D. (2012) Neuronal avalanches and coherence potentials. *Eur. Phys. J.-Spec. Top.*, **205** (1), 259–301.

43. Watson, H. and Galton, F. (1874) On the probability of the extinction of families. *J. Anthropol. Inst. Great Br.*, **4**, 138–144.

44. Athreya, K.B. and Jagers, P. (1997) *Classical and Modern Branching Processes, IMA*, Vol. 84, Springer.

45. Harris, T. (1963) *The Theory of Branching Processes*, Springer.

46. Kimmel, M. and Axelrod, D.E. (2002) *Branching Processes in Biology*, Springer.

47. Beggs, J. and Plenz, D. (2004) Neuronal avalanches are diverse and precise activity patterns that are stable for many hours in cortical slice cultures. *J. Neurosci.*, **24** (22), 5216–5229.

48. Levina, A., Ernst, U., and Herrmann, J.M. (2007a) Criticality of avalanche dynamics in adaptive recurrent networks. *Neurocomputing*, **70** (10-12), 1877–1881.

49. Otter, R. (1949) The multiplicative process. *Ann. Math. Stat.*, **20**, 248–263.

50. Turrigiano, G.G., Leslie, K.R., Desai, N.S., Rutherford, L.C., and Nelson, S.B. (1998) Activity-dependent scaling of quantal amplitude in neocortical pyramidal neurons. *Nature*, **391**, 892–896.

51. Bornholdt, S. and Rohlf, T. (2000) Topological evolution of dynamical networks: global criticality from local dynamics. *Phys. Rev. Lett.*, **84**, 6114–6117. doi: 10.1103/PhysRevLett.84.6114.

52. Bi, G. and Poo, M. (1998) Synaptic modification in cultured hippocampal neurons: Dependence on sike timing, synaptic strength and postsynaptic cell type. *J. of Neurosci.*, **18** (24), 10–464–10–472.

53. Shew, W., Yang, H., Yu, S., Roy, R., and Plenz, D. (2011) Information capacity and transmission are maximized in balanced cortical networks with neuronal avalanches. *J. Neurosci.*, **31** (1), 55–63.